JOURNAL OF MATERIALS SCIENCE 25 (1990) 3347–3358

Weldability of aluminium–lithium alloy 2090 using laser welding

P. A. MOLIAN
Department of Mechanical Engineering, Iowa State University, Ames, Iowa 50011, USA
T. S. SRIVATSAN
Department of Mechanical Engineering, University of Akron, Akron, Ohio 44325, USA

Lithium-containing aluminium alloys are of considerable current interest in the aerospace and aircraft industries because lithium additions to aluminium improve the modulus and decrease the density compared to conventional aluminium alloys. Many such alloys are under development for aircraft applications, which usually involves mechanical fastening. While aluminium–lithium alloys are fusion weldable with gas metal arc, gas tungsten arc and electron beam processes, they suffer from problems of weld porosity, heat-tearing cracking, poor penetration and low joint efficiency. In this paper, the weldability of aluminium–lithium alloys is briefly reviewed. The weldability of commercial aluminium–lithium alloy 2090 in the peak-aged condition was studied using laser welding. The quality of the welds was evaluated through mechanical tests (hardness and tensile tests) and microscopical observations. Mechanical property data and microscopical observations of the welds on prior surface-prepared (milled) material revealed a low degree of the weld surface degradation and an absence of porosity. This coupled with the attractive joint efficiencies suggest the superiority of the laser welding to conventional arc welding of this alloy. The performance of laser-welded butt joints is rationalized.

1. Introduction

The critical need for improved aircraft performance coupled with the implementation of "fail safe" and "safe-life" design concepts and an increased emphasis on damage tolerance resulted in the development of a number of new structural materials. In the race for the development of new structural materials to satisfy the requirements of: (a) lower density, (b) improved strength, (c) higher stiffness, (d) superior fatigue resistance and (e) durability, carbon-fibre-reinforced composites (CFC) and aluminium alloys have remained the two favourite contenders. Use of these alternative materials in aircraft structures, has, not surprisingly, been a slow and continuous process with rigorous testing, on the one hand, and large commercial investment, on the other, weighing heavily against any drive for change. The situation with carbon-fibre-reinforced composites involved their expensive manufacturing costs and difficult fabrication procedures. In addition, the very nature of a composite structure makes the description of a typical material suitable for comparative purposes difficult. Ingot metallurgy (IM) and powder metallurgy (P/M) aluminium alloys continue to remain as prime candidates for aircraft structures on account of their attractive manufacturing costs, their extensive previous use in airframe structures, and the availability of aluminium manufacturing facilities [1].

The lithium-containing aluminium alloys are emerging as a family of attractive lightweight alternatives to traditional high-strength aluminium alloys and carbon-fibre composites for use in aerospace, automotive and marine applications. These alloys offer a unique combination of properties, including high monotonic tensile and yield strengths, decreased densities, increased stiffness, good resistance to the propagation of fatigue cracks, and improved thermal stability coupled with the promise of attractive weight savings which would help to reduce operating costs by slimming down on fuel consumption. According to McDonnell Douglas, a 1% weight reduction translates to a 0.4% lower fuel usage. For a large commercial aircraft this results in fuel savings of around 33 000 gallons (~ 150 018 litres) a year. Another leading aerospace company projects that every kilogram shaved off the structural weight of a large aircraft is worth around $40 a year to the airline [2]. In recent years, these alloys have aroused considerable interest and have been the subject of increased research activity and several intensive investigations aimed at understanding their various metallurgical and mechanical characteristics [3–7]. Each increment of 1 wt % lithium alloyed with aluminium decreases the density by 3% and increases the elastic modulus (E) by about 6% [8]. The specific modulus (modulus of elasticity/weight) of an aluminium alloy with 2.8% lithium by weight is 21% higher than that of alloy 2024-T351 and 26% higher than that of aluminium alloy 7075-T651. The

0022–2461/90 $03.00 + .12

decrease in density is far more effective in reducing structural weight and increase savings in energy than improved strength, toughness or fatigue resistance [9]. For example, in an aluminium–3 wt % lithium alloy, structural weight savings of 10% on affected structures could be realized by direct substitution, and 16% by design modification [10].

Most high-strength aluminium alloys used in aircraft structures are mechanically fastened which has the drawbacks of slow assembly and limitations in joining thin sections. Fusion welding of lightweight aluminium–lithium alloys have been studied by a few investigators with a limited degree of success. However, there exists a need to develop new joining methods in order to extend the range of applications for these alloys and to improve the overall performance, durability, damage tolerance, and life of safety-critical components and structures. Furthermore, the new joining method could facilitate use of these alloys in marine hardware, lightweight pressure vessels and lightweight armoured vehicles.

The rationale for this work was to evaluate the weldability characteristics of the Al–2.7Cu–2.2Li–0.12Zr alloy 2090 joined by a high energy density source and to compare with conventional fusion welding processes. The quality of the laser welds was established through mechanical testing and microscopical observations of the weld. We begin with a review of previous studies on weldable lithium-containing aluminium alloys.

2. Weldability of aluminium–lithium alloys

There have been only a few studies to understand comprehensively the technique and use of welding to join lightweight aluminium–lithium alloys. Cross *et al.* [11] performed studies to evaluate the weldability of high-purity aluminium–lithium binary alloys using the varestraint test in order to assess their susceptibility to hot tearing. They observed the susceptibility of an alloy to hot tearing to vary with lithium content. Furthermore, the depth of penetration was found to increase with increasing heat input, as is observed in other aluminium alloys [12].

Cross *et al.* [11] also found the depth of penetration to increase with lithium concentration. The increase in penetration was rationalized as being due to the decrease in thermal conductivity that accompanies increasing lithium content. These researchers [11] observed the high-purity binary alloys to be: (a) readily weldable, and (b) have good resistance to hot tearing. Hot tearing is cracking in the weld zone caused by the inability of the liquid region to support the strain imposed by solidification shrinkage [11, 12].

Around the same time, Sperry and Mardigo [12] in Switzerland found lithium additions to aluminium to decrease electrical conductivity, which facilitates resistance of "spot" welding. The lithium was claimed to contribute to ductility and improve formability due to the fact that it exists in solid solution, and not as the coherent δ' (Al_3Li) precipitate. The δ' precipitate is detrimental to ductility because it promotes heterogeneous deformation, i.e. "planar slip" [14–17]. The alloy was found to be an attractive candidate for automotive applications in which spot welding is a cost-effective method of joining.

Tungsten-inert-gas (TIG) welding studies of the ternary Al–4.5Cu–1.1Li–0.5Mn–0.2Cd alloy 2020 developed by Alcoa revealed the butt joints to have low weld strengths of only 230 MPa in comparison with parent material tensile strength of 580 MPa [18]. However, heat treatment of the weldments was found to restore the strength of the weld to about 500 MPa. Other studies to attempt to weld alloy 2020 made by rapid solidification resulted in a large amount of porosity coupled with the weldments experiencing grain-boundary liquation at the fusion line [19]. The problems associated with welding the rapidly solidified 2020 alloy were rationalized as being not the result of alloy composition but more a consequence of powder processing and degassing.

The advantage of rapid solidification in producing superior alloys is well documented in the literature [20, 21]. Rapid solidification processing in combination with powder metallurgical (P/M) consolidation techniques offers potential improvements in the properties of lithium-containing aluminium alloys. Bowden and Meschter [22] investigated the weldability of a series of rapidly solidified, powder metallurgy processed binary and ternary aluminium alloys containing 3 wt % lithium. In their study, Bowden and Meschter fabricated alloys from vacuum-atomized powder, and the welding was performed in the as-extruded (i.e. F) temper. Electron beam bead-on plate welds were made using a beam current of 125 mA, an accelerating voltage of 15 V, and a welding speed of 0.18 m sec^{-1}. The welded plates were heat treated to peak strength and tensile tests were performed. Results of the tensile tests performed on the as-welded plates were compared with similar tests performed on peak-strength plates that were not welded. The joint efficiencies ranged from about 60% to 75% of base material properties. These researchers [22] rationalized the degradation in strength in the weld zone to be the result of destruction of the substructure caused by the melting that accompanies welding. Because substructure contributions to strength are significant in the case of P/M alloys, destruction of the substructure that results from the thermomechanical processing used to form the product directly results in a degradation in strength. The essential outcome of the study by Bowden and Meschter was that the RS-P/M Al–Li–X alloys are weldable with the binary aluminium–3 wt % lithium alloys containing zirconium exhibiting joint efficiencies as high as 75%.

A survey of the published literature on weldable lithium-containing aluminium alloys reveals the Soviet alloy 01420 (Al–5Mg–2Li–X) to be the only lightweight aluminium–lithium alloy in widespread commercial use. Alloy 01420 was developed in 1967 by Fridlyander [23] and its density (2.47 g cm^{-3} [24]) is lower that that of other high-strength commercial aluminium alloys. Mironenko and co-workers [25, 26] conducted detailed investigation to evaluate the fusion weldability of 01420 and found the alloy to have "good weldability" [25]. They also found that filler

materials containing various amounts of manganese, titanium, zirconium or chromium provided stronger joints than those produced by the parent filler material. Fridlyander [27], in a study on the weldability of aluminium alloy 01420, obtained joint efficiencies (i.e. strength of the weld divided by strength of the parent material) of 70% without post-weld heat treatment and as high as 99.5% after post-weld heat treatment, i.e. re-solutionizing, air-cooling and artificial ageing. Joint efficiencies of 80% for TIG welding were obtained for welds that received no post-weld heat treatment using an Al–6.3Mg–0.5Mn–0.2Zr filler alloy. However, numerous other studies by Soviet researchers revealed weld-zone porosity to be a key problem with alloy 01420 [26, 28, 29]. The high porosity was attributed to the surface reactivity of the alloy with ambient moisture resulting in the formation of lithium-containing compounds such as lithium oxide (LiO_2), lithium hydroxide (LiOH), lithium carbonate (Li_2CO_3) and lithium nitride (LiN). In the case of an Al–Mg–Li alloy, Fridlyander found these phases to produce absorption of ambient moisture on to the alloy surface, resulting in hydrogen penetrating into the weld pool. To minimize weld-zone porosity, pre-welding surface preparation was found to be essential [26, 30]. Fedoseev *et al.* [30], following a systematic study of surface preparation techniques, found that mechanically milling 0.5 mm from the alloy surface of chemically milling 0.3 mm from the surface in a 200 g l^{-1} alkaline aqueous solution, reduced weld-zone porosity to acceptable levels.

Other research efforts found the Soviet alloy 01420 to be weldable and that "good" joint efficiencies could be easily obtained provided adequate care was taken during surface preparation prior to welding. This was to ensure removal of the hydrated layer that forms on the surface. Most recently, Pickens *et al.* [31] investigated the weldability of the Soviet-developed Al–5%Mg–2%Li–0.1%Zr alloy 01420 using TIG welding and found the alloy to be weldable with tensile strength joint efficiencies as high as 64% when using base-material filler, and without post-weld heat treatment. With post-weld heat treatment of the alloy, tensile strength joint efficiencies as high as 85% were obtained. The susceptibility of the alloy to weld-zone porosity was minimized to acceptable levels by either machining or by chemical milling in a 30% NaOH solution followed by rinsing inn 30% nitric acid at 50–60° C. The softening of the weld bead with respect to the base materials was attributed to the effects of lithium depletion in the weld bead when using base-material filler, coupled with microstructural coarsening.

A brief survey of the available literature on weldability of the lithium-containing aluminium alloys reveals that these alloys are weldable and high joint efficiencies can be obtained for material that is re-heat treated after welding.

3. Materials and methods

3.1. Material

The aluminium–lithium alloy 2090 of composition (wt %) 2.8% copper, 2.05% lithium, 0.12% zirconium, 0.02% iron, 0.0% silicon, 0.0% magnesium, 0.02% titanium, and balance aluminium, was provided by Alcoa laboratories (Pennsylvania, USA) in the near peak-aged T8E41 condition. The designation T8E41 refers to an experimental temper involving solution heat treatment at 549° C for 2 h and water quenching. The as-quenched material was then deformed 6% in tension in order to relieve the residual stresses resulting from quenching and to facilitate heterogeneous nucleation of precipitates during subsequent artificial ageing. The alloy was aged for 24 h at 163° C [32].

3.2. Microstructural characterization

Optical metallography samples were cut from the three orthogonal directions of the as-received plate. The samples were mounted in bakelite and wet ground on 320, 400 and 600 grit silicon carbide paper using water as lubricant and then mechanically polished with 1 and 0.05 μm alumina-based lubricant. Grain morphology was revealed using Keller's etch and observed in an optical electron microscope.

3.3. Laser welding

Two types of laser welding were performed that included bead-on-plate and butt-joint. A continuous wave CO_2 laser at a power level of 1.3 kW was used to join 1.6 mm thick plates of 2090-T8E41 alloy. A 191 mm focal length lens was employed to focus the beam at 7.6 mm distance away from the specimen surface. The weld speed was varied from 42.33 to 254 mm sec^{-1}. An argon cover gas at a pressure of 10 p.s.i. was used to shield the weld from the atmosphere during welding. The bead-on-plate welds performed with no complete penetration. A multipass laser welding method was used to obtain a fully penetrated butt joint.

An important variable in the weldments was the initial surface condition. Welding was performed on both the as-received condition and the mechanically milled condition. Mechanical milling removed a layer of 0.127 mm from each side. The joint gap for the square-butt weld was made between 0.0254 and 0.254 mm.

3.4. Robot-aided MIG welding

Conventional metal-inert gas arc welding (MIG) was also conducted using a General Electric P50 robot and 4047 (Al–12%Si) filler metal. Both bead-on-plate and square-butts were carried out. The specimens were surface milled prior to arc welding.

3.5. Analysis of welds

The welds were sectioned, metallographically polished and etched using Keller's agent. A high resolution optical electron microscope was used to examine the weld quality that included porosity, hot tearing and the extent/depth of penetration. A Vicker's microhardness tester was used to determine the hardness at various locations along the weld at a load of 100 g. Tensile tests were performed on the base material and the as-welded butt welds using a 100 000 N capacity electromechanical machine. Multiple tests were conducted in order to ensure consistency in results.

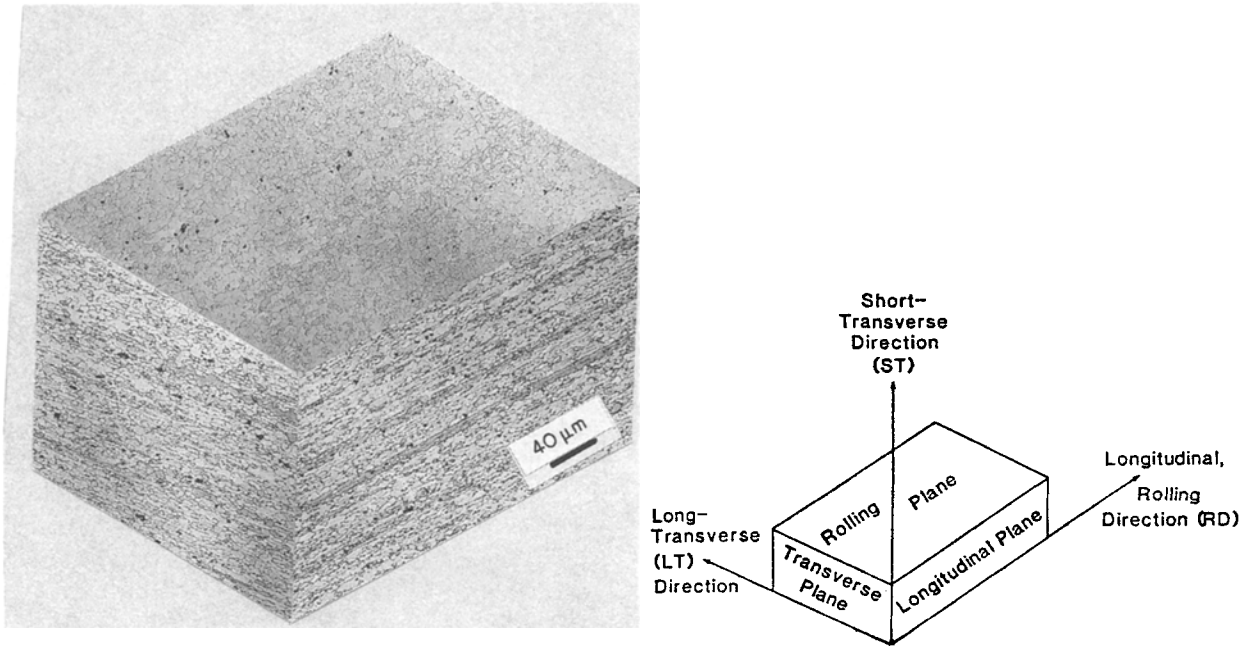

Figure 1 Triplanar optical micrograph illustrating the grain structure of the Al–Li–Cu–Zr alloy plate 2090.

4. Results and discussion

4.1. Microstructure

Optical microscopy of the as-received 2090 alloy in the T8E41 condition revealed the material to be anisotropic, having an unrecrystallized microstructure, with large pancake shaped grains elongated in the longitudinal direction, as a consequence of deformation introduced during rolling. A triplanar optical micrograph illustrating the grain structure of the material in the three orthogonal directions is shown in Fig. 1. Previous transmission electron microscopy studies on this alloy in the T8E41 condition revealed that strengthening in the peak-aged condition was due to the presence of ordered, coherent, spherical precipitates of δ' (Al_3Li) and the plate-like precipitates T_1 (Al_2CuLi) (along the (1 1 1) habit planes) and θ' (Al_2Cu) (along the (1 0 0) habit plane). Fig. 2 shows a typical (1 0 0) electron diffraction pattern for the ternary alloy. The superlattice spots are due to the δ' phase and the satellite spots due to the T_1 precipitates. Nucleation of the T_1' and T_1 phases is accelerated by the deformation induced prior to ageing. The metastable T_1' precipitate is thought to be a precursor to the hexagonal T_1 phase. As a consequence of the 6% stretch prior to ageing, the precipitates are distributed homogeneously within the grains, and suppressed along the grain boundaries.

Additional strengthening contributions to this alloy result from the β' (Al_3Zr) phase. The cubic β' precipitate also known as dispersoid has an $L1_2$ structure and nucleates heterogeneously on dislocations and grain boundaries [33, 34]. The β' phase is coherent with the aluminium matrix and aids in: (i) retarding subgrain boundary migration and coalescence, (ii) suppresses recrystallization, controls grain growth and stabilizes the subgrain structure [35, 36]. The elements iron (0.02%) and silicon (0.01%) are present as impurities. During ingot solidification and subsequent processing,

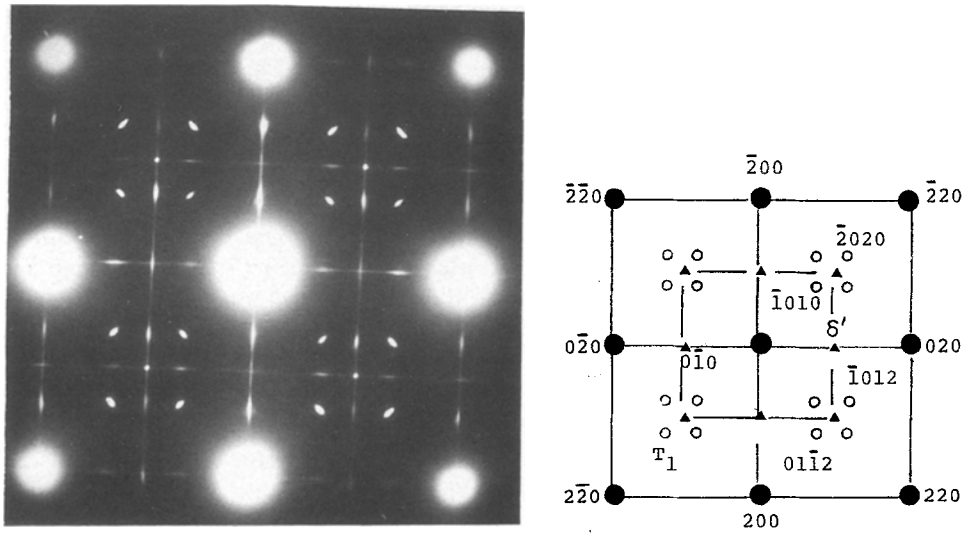

Figure 2 A typical (0 0 1) selected-area diffraction pattern of Al–Li–Cu alloys. Superlattice spots are caused by the T_1 and δ' reflections. Zone axis: matrix (0 0 1); T_1 precipitate (2423).

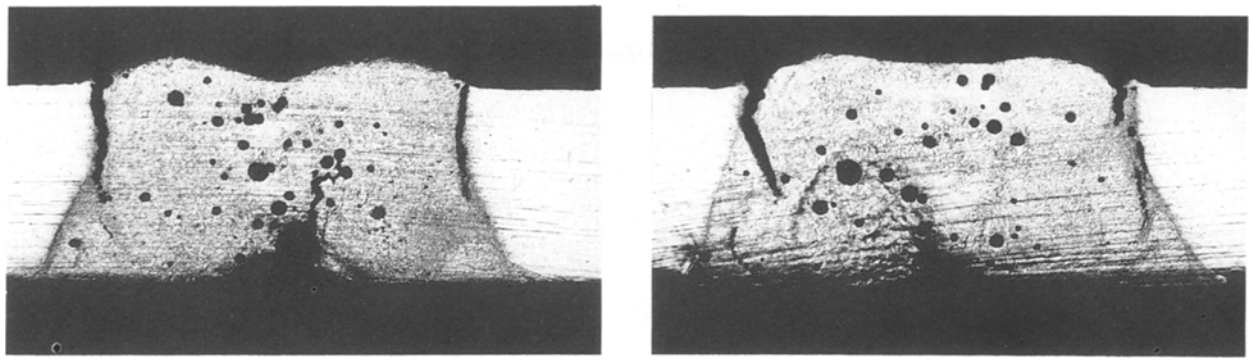

Figure 3 Optical micrographs showing transverse section of MIG-welded 2090 alloy.

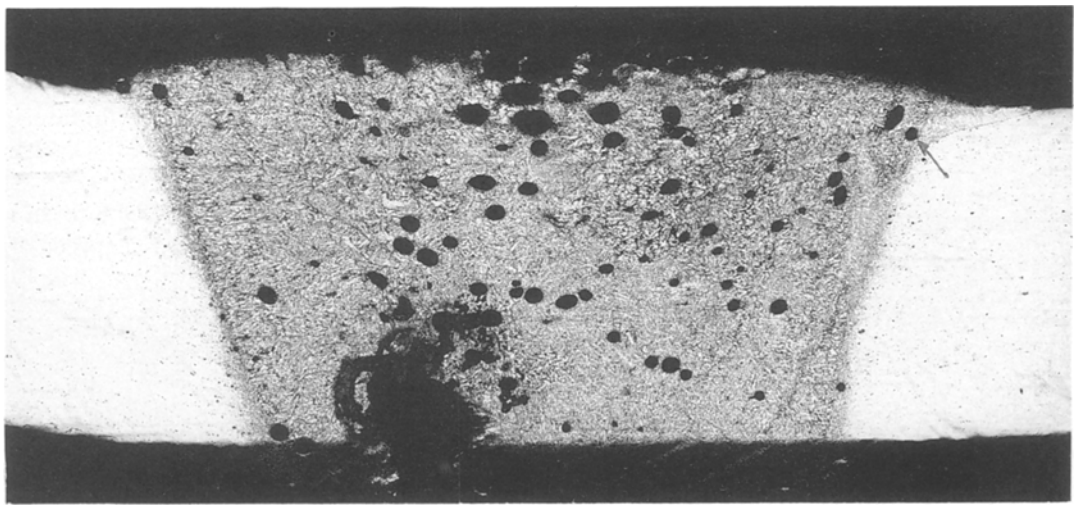

Figure 4 Optical micrograph showing transverse section of the MIG-welded 2090-T8E41 alloy, ×300.

these impurity elements precipitate out as the insoluble constituent phase identified as Al_7Cu_2Fe by selected-area diffraction [37].

4.2. Metal inert gas (MIG) welding

Fig. 3 shows the transverse sections of bead-on-plate welds at two different speeds showing porosity in the middle and hot-tearing at the boundary of the weld zone. A square butt joint with the addition of 4047 filler metal is shown in Fig. 4, enlarged the width, and eliminated hot-tearing due to change in composition of the weld zone.

4.3. Laser welding

Two mechanisms, namely "deep penetration" and "conduction" are involved in laser welding depending on the laser parameters (Fig. 5). A deep penetration weld is characterized by an hour-glass shape with a high depth-to-width ratio. Deep penetration is normally accompanied by: (a) excessive melting, (b) loss of material through vaporization, (c) low cooling rate, (d) shrinkage cracks, and (e) gas porosity. These effects are the result of the formation of a "key hole" with concomitant energy transfer through the key-hole. In contrast, a conduction weld exhibits a small

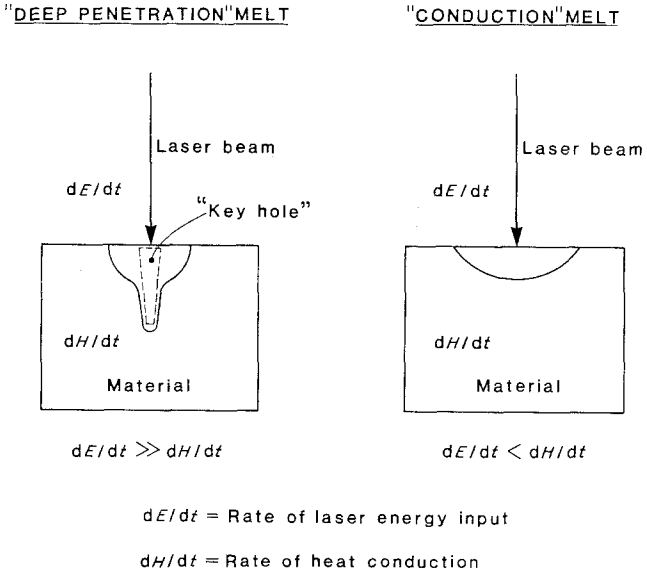

Figure 5 Schematic representation of deep penetration and conduction welds.

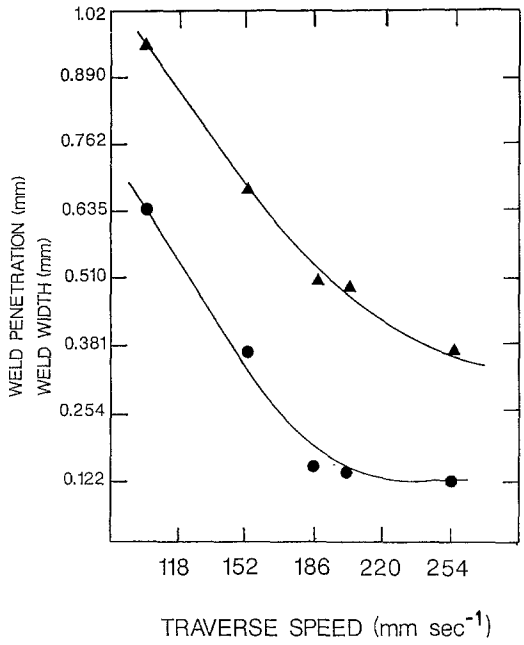

Figure 6 Effect of weld travel speed on (●) weld penetration and (▲) weld width.

depth-to-width ratio and a low degree of defects. The geometry of a conduction weld is hemispherical and is similar to that of conventional arc welds.

The effect of laser weld traverse speed on weld depth (penetration) and weld width for bead-on-plate (BOP) welds that received no prior surface preparation is shown in Fig. 6. As expected, both weld depth (penetration) and weld width decreased exponentially, with a decrease in traverse speed indicating a transition from deep penetration to conduction weld. Transverse sections of bead-on-plate weld profile is shown in Fig. 7. Few pores were observed mostly near the weld/base material interface. The amount of porosity was observed to be unaffected by the depth of penetration. In all cases, the heat-affected zone (HAZ) was found to be negligible. The microhardness of the welds were found to be in the range 85 to 90 $kg\,mm^{-1}\,mm^{-1}$ irrespective of the traverse speed of the laser, while the hardness of the base material was 140 $kg\,mm^{-1}\,mm^{-1}$ and the heat-affected zone hardness was 110 $kg\,mm^{-1}\,mm^{-1}$, respectively. The microstructures of the bead-on plate (BOP) welds processed at speeds of 102 and

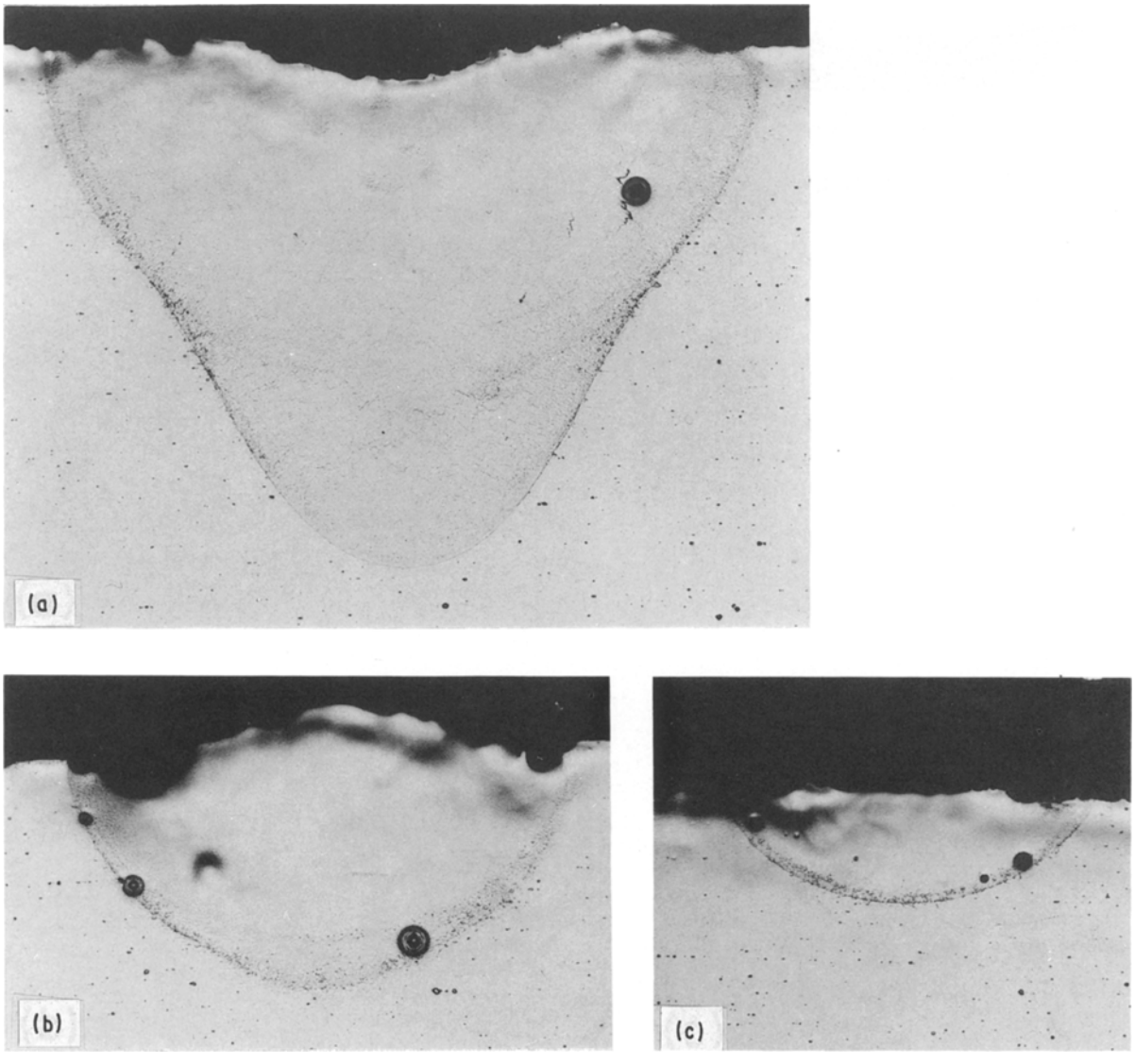

Figure 7 Transverse sections of bead-on-plate weld profiles, ×40.

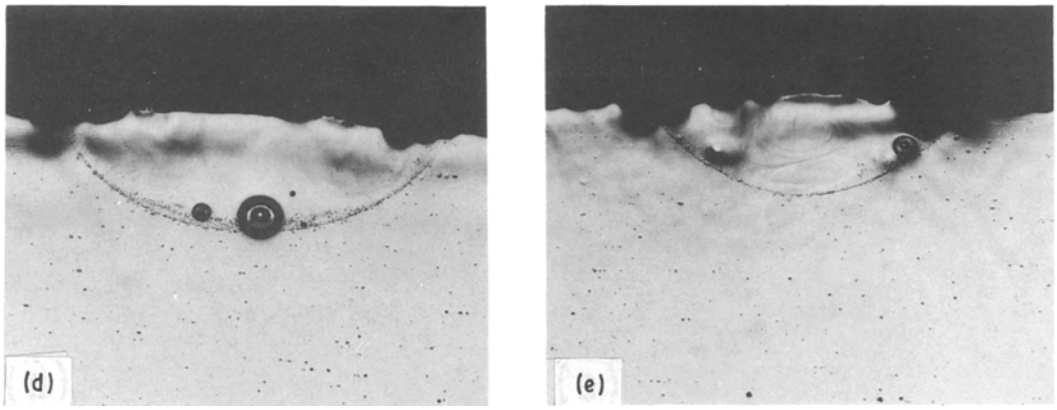

Figure 7 Continued

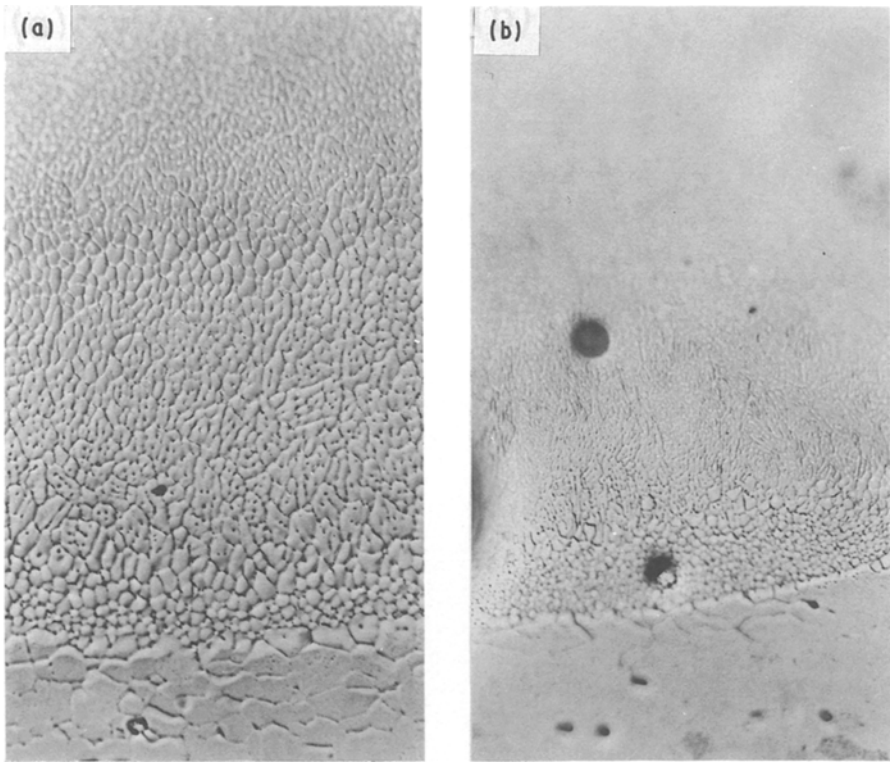

Figure 8 Microstructures of bead-on-plate welds, ×800. Traverse speed: (a) 102 mm sec^{-1}, (b) 203 mm sec^{-1}.

203 mm sec^{-1} are shown in Fig. 8. The optical micrographs reveal cellular structures with the presence of fine precipitates or particles inside the cells. The fineness of the cell structure decreased as the distance from the surface into the bulk material increased. Extremely fine and almost featureless structures were observed as the traverse speed was increased.

Micrographs of the transverse sections of the laser butt-joints are shown in Figs 9a and b. Table I summarizes the conditions under which the welds shown in this figure were produced. Weld penetration in the butt joint (0.51 mm) was found to be greater than that of the bead-on-plate welds (0.76 mm) for a traverse speed of 127 mm sec^{-1}. The observed difference in

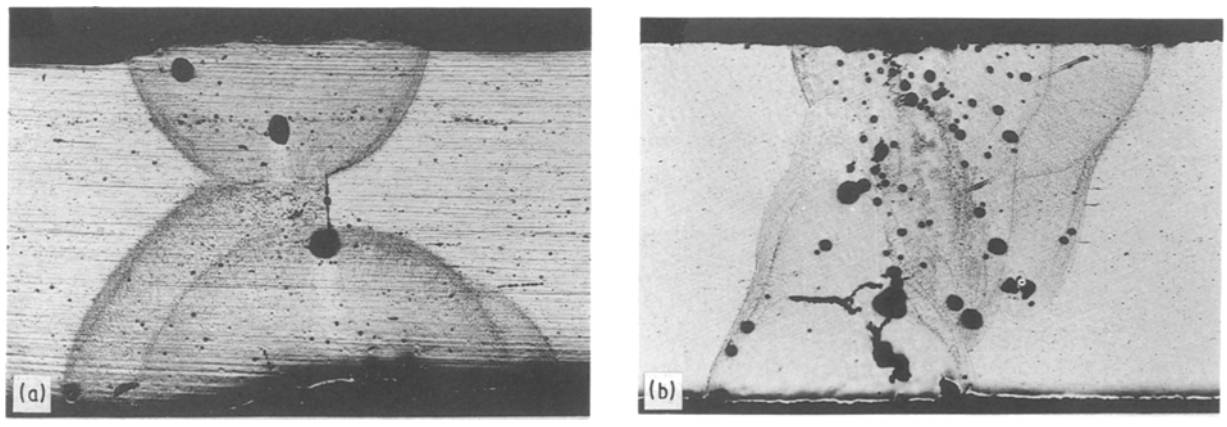

Figure 9 Transverse sections of square-butt joints, ×40.

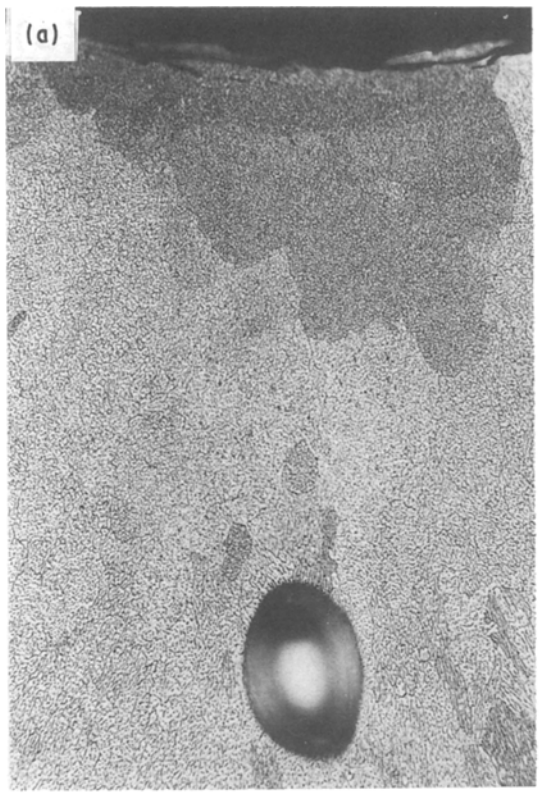

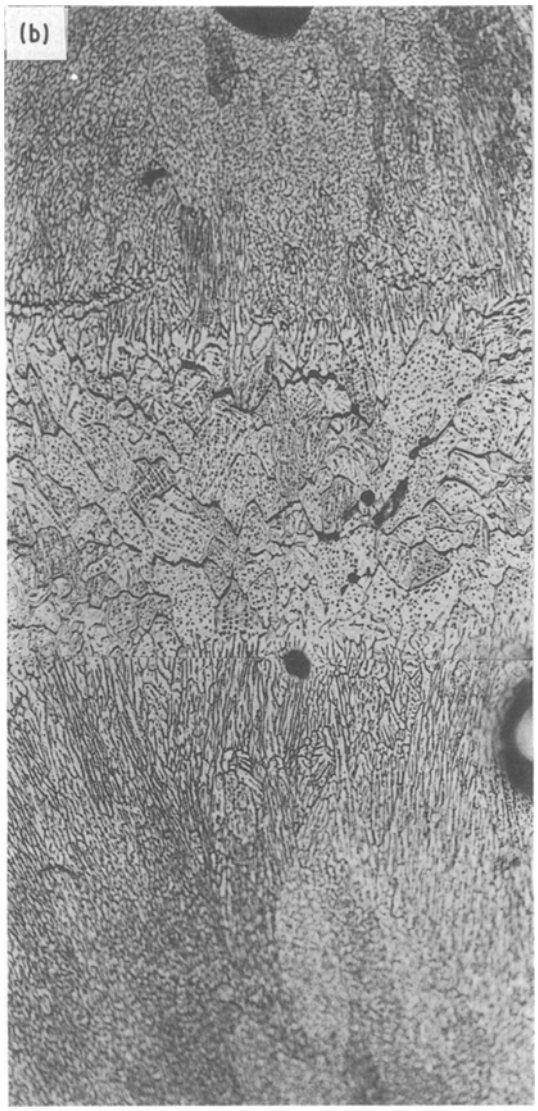

Figure 10 Various regions in the transverse section of butt-joint of Fig. 9a, ×250. (a) and (c) Top and bottom of weld, (b) middle of the weld.

penetration is attributed to trapping of the laser beam in the butt-joint gap and the subsequent internal reflections within the gap in the case of butt welds. For mechanically milled surfaces, the laser traverse speed was reduced (42.33 mm sec^{-1}) on account of the higher reflectivity of the surface. Fig. 9 shows the significant effect of surface preparation on weld porosity.

The microstructures of the laser weld in various locations of the transverse section (Fig. 9a) are shown in the micrographs in Figs 10 and 11. It is evident from the electron micrographs that fine cellular-dendritic structures are present near the surface of the weld. As the distance from the sufrace into the bulk material increases, the intrinsic microstructural features, namely, grain size and second-phase particle size become larger. The transition from a fine structure to a coarse structure coupled with the formation of particles is rationalized on the basis of solidification mechanics. The solidification growth rate (R) and temperature gradient (G) are two key parameters along with solute concentration which determine the type and fineness of structures in the weld zone. (The solidification pattern is seen better at the weld/base material interface, as shown in Fig. 10). The fine cellular structure at the base material/weld interface is

TABLE I Laser welding conditions

	Fig. 7a	Fig. 7b
Surface preparation	None	Mechanical milling
Traverse speed (mm sec^{-1})	42.33	127.00
Weld procedure	Both sides	Both sides

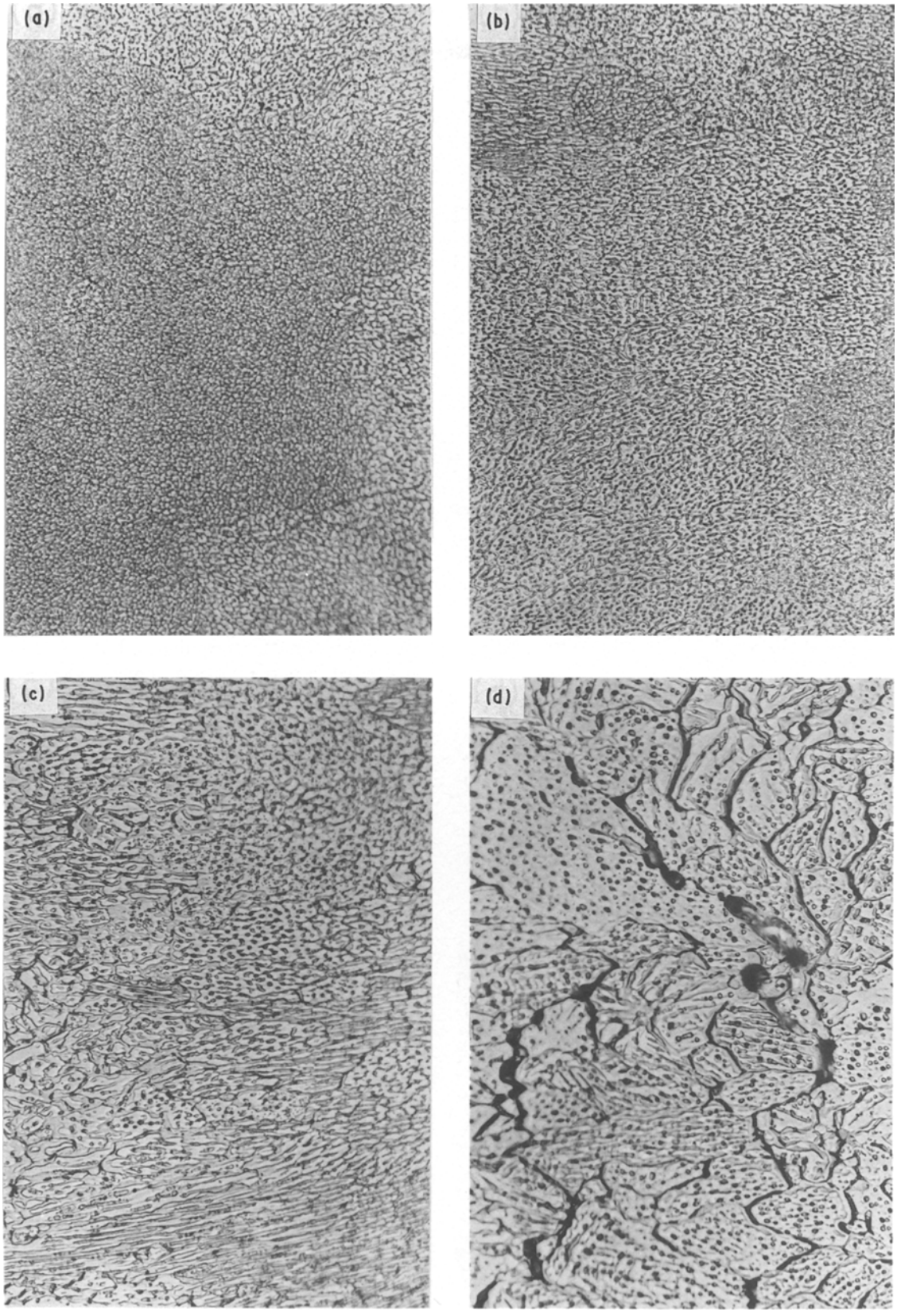

Figure 11 Microstructures of the butt-joint of Fig. 9b, ×500. (a) Near the surface, (b) subsurface, (c) near the middle, (d) middle.

largely due to the large G/R ratio. Epitaxial growth from the cells to form cellular structures coupled with the presence of fine cellular structures in the middle are seen in the optical micrograph in Fig. 12. In contrast to laser welding, MIG welding resulted in coarse microstructures (Fig. 13).

Hardness of the laser weld was found to be 85 to 90 $kg\,mm^{-1}\,mm^{-1}$ irrespective of the location of the weld (Fig. 14). The hardness values (numbers) were consistent and clearly unaffected by the presence of the various microstructural features resulting from welding.

Tensile tests were conducted to identify the specific influence of weld microstructure on joint tensile strength and weld joint efficiency. The ultimate tensile strength (UTS) obtained for the 2090-T8E41 alloy in the as-received condition and in the welded condition is summarized in Table II. The ultimate tensile

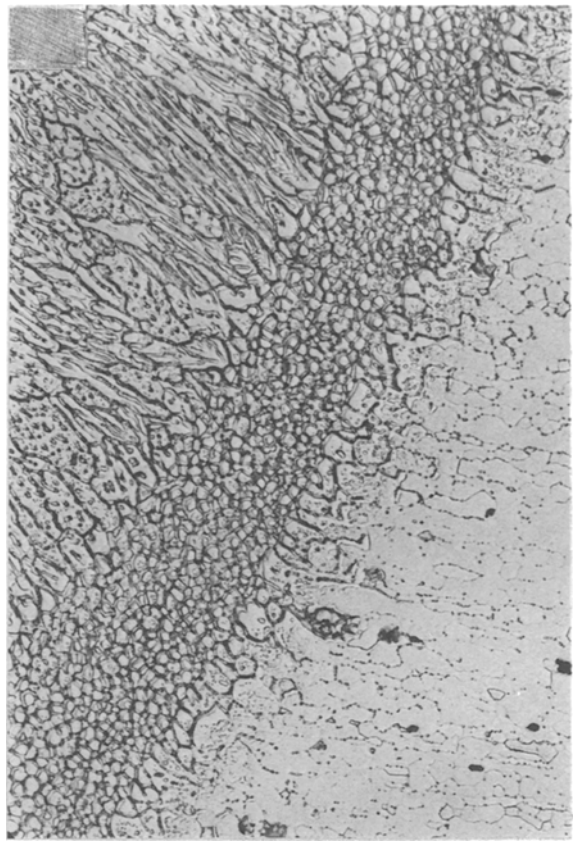

Figure 12 Microstructures at the weld/base-metal interface, × 500.

strength in the longitudinal (L) orientation (408 MPa) was 25% greater than in the transverse (LT) orientation (302 MPa) (Table III). The tensile strength of the as-welded material was lower than that of the as-received, unwelded material. However, tensile strength of the butt-weld with prior surface preparation (335 MPa) was better than the strength of the weld with no prior surface preparation (225 MPa).

TABLE II Properties of the welded material

Alloy and temper	Condition	Ultimate tensile strength		Tensile strength joint efficiencies (%)
		MPa	10^3 p.s.i.	
2090-T8E41 (as-received)	No prior surface preparation	225	33	55.10
2090-T8E41	With prior preparation	335	49	82.10

Tensile strength joint efficiencies for the welded conditions were measured shortly after welding. The joint efficiency values were calculated and then compared with data obtained by Martukanitz *et al.* [38] using other fusion welding processes on alloy 2090-T8E41. Fig. 15 highlights the comparison in joint ultimate tensile strength between laser welding and other welding procedures used for this alloy. It should be noted that conventional weld processes used a filler metal of the type 4043, 4047, 4145 and 2319. The improved joint efficiency obtained for the laser weld is attributed in part to: (a) the small heat-affected zone size, and (b) the fine structures in the weld zone.

5. Conclusions

The general conclusions of the present study on the weldability of aluminium–lithium alloy 2090 are summarized as follows.

1. Alloy 2090 is indeed weldable using a high energy beam source (laser) and tensile strength joint efficiencies

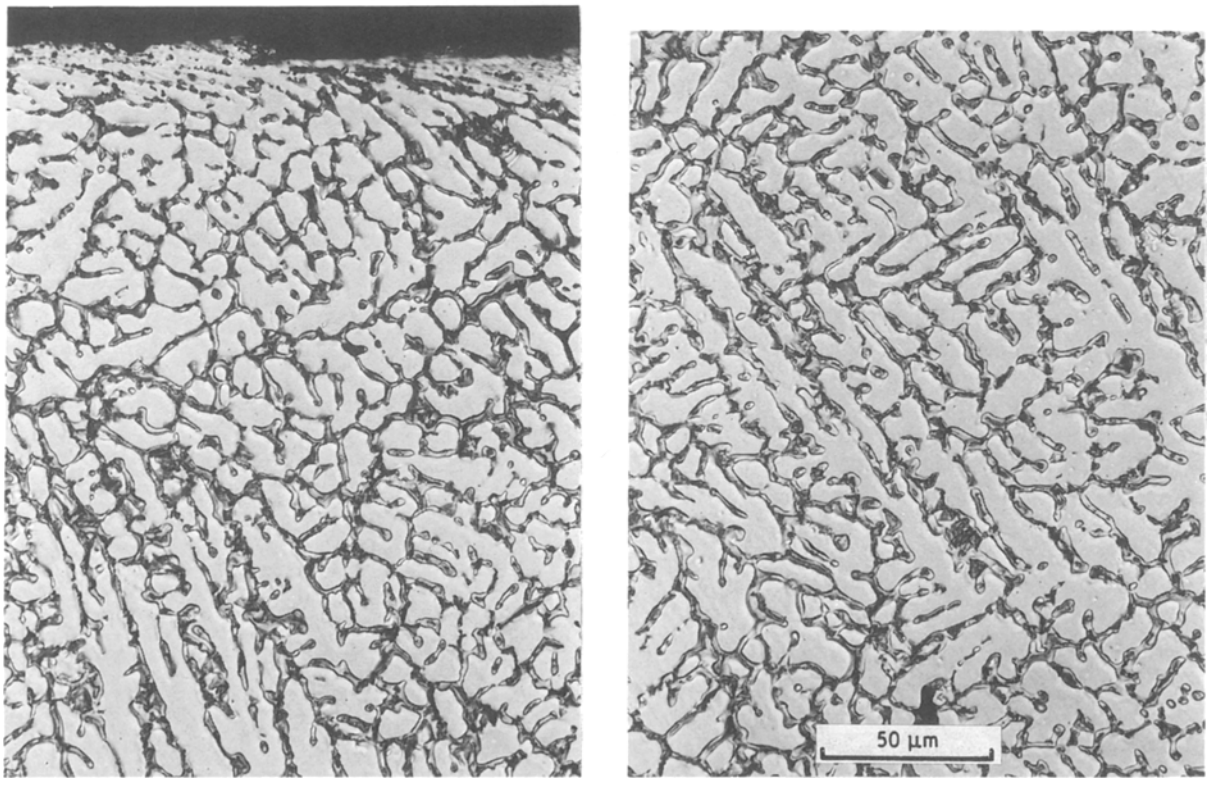

Figure 13 Optical micrograph showing coarse microstructures resulting from MIG welding.

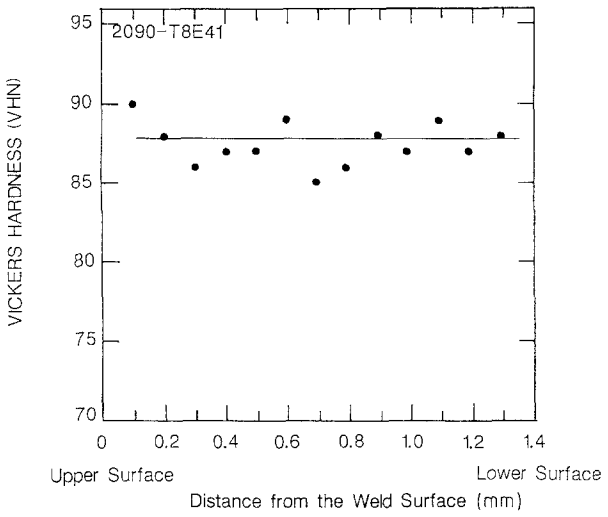

Figure 14 Vickers hardness profile across transverse section of laser weldments in the as-welded condition.

of 55% were obtained with no prior surface preparation on the as-received material. By subjecting the as-received material to surface preparation, the tensile strength joint efficiencies could be increased to as high as 82%.

2. Hardness (numbers) of the laser weld were found to be consistent and around 85 to 90 $kg\,mm^{-1}\,mm^{-1}$, and unaffected by the presence of various microstructural features resulting from welding.

3. As a result of using a laser, fine cellular-dendritic structures result near the surface of the weld. The intrinsic microstructural features coarsen or become larger as the distance from the surface into the bulk material increases. This transition is rationalized on the basis of solidification mechanics.

4. Weld depth (penetration) and weld width decreased exponentially, with a decrease in traverse speed of the laser beam, indicating a transition in mechanism from deep penetration to conduction weld.

5. Only few pores were observed on the weld/base material interface and the degree of porosity of the laser weld was observed to be unaffected by the depth of penetration.

Acknowledgements

The authors thank Mr R. P. Martukanitz, Alcoa Laboratories, for providing sheets of the alloy, and Mr Didi Widjaja for experimental assistance during the course of this study. This work was partially supported by Iowa State University and the University of Akron through Faculty Research Grant No. 1034. Thanks also to Ms Karen Ober for her assistance in the preparation of this manuscript.

TABLE III Properties of base material

Alloy and temper	Orientation	Ultimate tensile strength	
		MPa	10^3 p.s.i.
2090-T8E41 (as-received)	Longitudinal	408	59
2090-T8E41 (as-received)	Transverse	302	44

References

1. E. J. LAVERNIA, B. POGGINLI, I. SERVI, J. CLARK, F. KATRAK and N. J. GRANT, *J. Metals* **37** (11) (1985) 35.
2. JOHN MACK, *Materials Edge* (7) (1988) 23.
3. T. H. SANDERS Jr and E. A. STARKE Jr, (Eds) "Aluminum–Lithium Alloys: Proceedings of the First International Conference on Aluminum–Lithium Alloys" (Metallurgical Society of AIME, Warrendale, Pennsylvania, 1981).
4. *Idem*, "Aluminum–Lithium Alloys II: Proceedings of the Second International Conference on Aluminum–Lithium Alloys", (Metallurgical Society of AIME, Warrendale, Pennsylvania, 1984).
5. C. A. BAKER, P. J. GREGSON, S. J. HARRIS and C. J. PEEL (Eds), "Aluminum–Lithium Alloys III: Proceedings of the Third International Conference on Aluminum–Lithium Alloys" (The Institute of Metals, London, 1986).
6. E. A. STARKE Jr and T. H. SANDERS Jr (Eds) "Aluminum Alloys: Their Physical and Mechanical Properties, Proceedings of the First International Conference on Aluminum Alloys" (EMAS, London 1986).
7. "Aluminum–Lithium Alloys IV: Proceedings of the Fourth International Conference on Aluminum–Lithium Alloys", France (1987) in press.
8. K. K. SANKARAN and N. J. GRANT, in "Aluminum–Lithium Alloys", edited by T. H. Sanders Jr and E. A. Stark Jr (Metallurgical Society of AIME, Warrendale, Pennsylvania, 1981) p. 206.
9. V. WIGOTSKY, *Aerospace Amer.* June (1984) 74.
10. W. E. QUIST, G. H. NARAYANAN and A. L. WINGERT, in "Aluminum–Lithium Alloys II," T. H. Sanders Jr and E. A. Starke Jr (Metallurgical Society of AIME, Warrendale, 1984) p. 313.

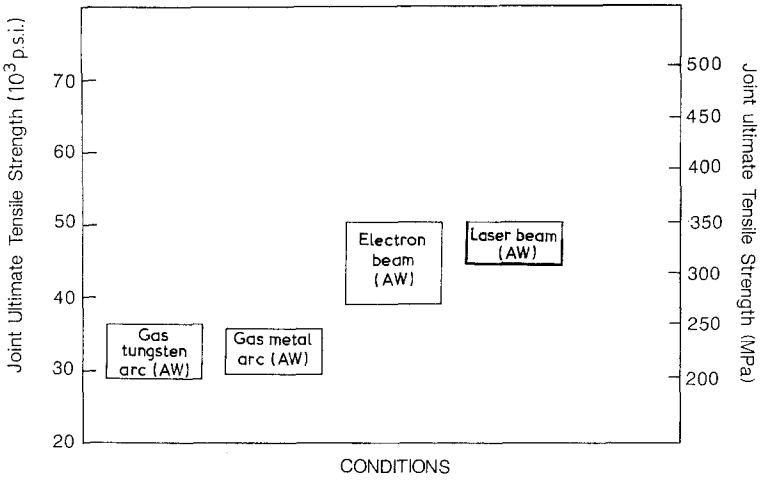

Figure 15 Joint tensile strength as a function of weld condition.

11. C. E. CROSS, D. L. OLSON, G. R. EDWARDS and J. F. CAPES *ibid.* p. 675.
12. "Welding Aluminum" (The Aluminum Welding Society, Miami, Florida, 1972)
13. P. R. SPERRY and F. N. MARDIGO, Brit Pat 1 572 587 (1980).
14. E. A. STARKE Jr, T. H. SANDERS Jr and I. G. PALMER, *J. Metals* **33** (8) (1981) 24.
15. T. H. SANDERS Jr, in "Aluminum–Lithium Alloys II", edited by T. H. Sanders Jr and E. A. Starke Jr (Metallurgical Society of AIME, Warrendale, Pennsylvania, 1981) p. 63.
16. T. H. SANDERS Jr and E. A. STARKE Jr *Acta Metall.* **30** (1982) 927.
17. E. A. STARKE Jr and F. S. LIN, *Met. Trans.* **13A** (1982) 2259.
18. M. HOLT and J. A. NOCK, Jr, *Prod. Eng* August (1960) p. 38.
19. C. A. ZANIA and W. A. PALKO, Report No DINSRDC/SME-84/37. DARPA order 4872 (Defense Advanced Research Projects Agency, Washington DC, 1984).
20. J. R. PICKENS, *J. Mater. Sci.* **16** (1981) 1437.
21. F. H. FROES and J. R. PICKENS, *J. Metals* **36** (1984) 14.
22. D. M. BOWDEN and P. J. MESCHTER, *Scripta Metall.* **18** (1984) 963–968.
23. I. N. FRIDLYANDER, Brit. Pat. 1 172 736 (February 1967).
24. I. N. FRIDLYANDER, S. M. AMBARTSUMYAN, N. V. SHIRYAYEVA and R. M. GABIDULLIN, *Metal. Oved. Term. Met.* (3) (1968) 211.
25. V. N. MIRONENKO, V. S. EVSTIFEEV and S. A. KURSHUNKKOVA, *Weld Prod.* **24** (12) (1977) 44.
26. V. N. MIRONENKO and A. I. LITVINTSEV, *ibid.* **26** (1) (1979) 30 (English translation).
27. I. N. FRIDLYANDER, *Met. Sci. Heat Treat. Metall.* **3** (1975) 240.
28. C. A. BOKSHTEIN, *Automatic Welding*, **6** (1978) 34.
29. A. YA. ISHCHENKO, *ibid.* **32** (2) (1979) 18.
30. V. A. FEDOSEEV, V. I. RYAZANSEV, N. V. SHIRYAESA and YU. P. ARBUZOV, *Weld. Prod.* **12** (1979) 19.
31. J. R. PICKENS, T. J. LANGAN and E. BARTA, in "Aluminum–Lithium Alloys III", edited by C. A. Baker, S. J. Harris and C. J. Peel (The Institute of Metals, London, 1986) p. 137.
32. R. J. RIOJA, P. E. BERTZ, R. R. SAWTELL, W. H. HUNT and E. A. LUDWICZAK, in "Aluminum Alloys: Their Physical and Mechanical Properties", First International Conference, Charlettesville, Virginia, edited by E. A. Starke Jr and T. H. Sanders Jr (EMAS, London, 1986).
33. E. NESS and N. RYUM, *Scripta Metall.* **5** (1971) 987.
34. R. J. RIOJA and E. A. LUDWICZAK, in "Aluminum–Lithium III", Proceedings of the Third International Conference on Aluminum–Lithium Alloys, edited by C. A. Baker, C. J. Peel, P. J. Gregson and S. J. Harris (Institute of Metals, London, 1986) p. 471.
35. J. M. GALBRAITH, M. H. TOSTEN and P. R. HOWELL, *J. Mater. Sci.* **22** (1987) 27.
36. T. S. SRIVATSAN and T. A. PLACE, *J. Mater. Sci.*, **24** (1989) 1543–1551.
37. A. MUNITZ, A. ZANGVIL and M. METZGER, *Metall. Trans.* **11A** (1980) 1863.
38. R. P. MARTUKANITZ, C. A. NATALIE and J. O. KNOEFEL, *J. Metals,* November (1987) 38.

Received 4 January
and accepted 17 August 1989